The Astrophysical Journal, 691:175–181, 2009 January 20 doi:10.1088/0004-637X/691/1/175

A SEARCH FOR A DARK MATTER ANNIHILATION SIGNAL TOWARD THE CANIS MAJOR OVERDENSITY WITH H.E.S.S.

F. Aharonian[1,2], A. G. Akhperjanian[3], U. Barres de Almeida[4,29], A. R. Bazer-Bachi[5], B. Behera[6], W. Benbow[1], K. Bernlöhr[1,7], C. Boisson[8], V. Bochow[1], V. Borrel[5], I. Braun[1], E. Brion[9], J. Brucker[10], P. Brun[9], R. Bühler[1], T. Bulik[11], I. Büsching[12], T. Boutelier[13], S. Carrigan[1], P. M. Chadwick[4], A. Charbonnier[14], R. C. G. Chaves[1], A. Cheesebrough[4], L.-M. Chounet[15], A. C. Clapson[1], G. Coignet[16], L. Costamante[1,30], M. Dalton[7], B. Degrange[15], C. Deil[1], H. J. Dickinson[4], A. Djannati-Ataï[17,31], W. Domainko[1], L. O'C. Drury[2], F. Dubois[16], G. Dubus[13], J. Dyks[11], M. Dyrda[18], K. Egberts[1], D. Emmanoulopoulos[6], P. Espigat[17], C. Farnier[19], F. Feinstein[19], A. Fiasson[19], A. Förster[1], G. Fontaine[15], M. Füssling[7], S. Gabici[2], Y. A. Gallant[19], L. Gérard[17], B. Giebels[15], J. F. Glicenstein[9], B. Glück[10], P. Goret[9], C. Hadjichristidis[4], D. Hauser[1], M. Hauser[6], S. Heinz[10], G. Heinzelmann[20], G. Henri[13], G. Hermann[1], J. A. Hinton[21], A. Hoffmann[22], W. Hofmann[1], M. Holleran[12], S. Hoppe[1], D. Horns[22], A. Jacholkowska[19], O. C. de Jager[12], I. Jung[10], K. Katarzyński[23], S. Kaufmann[6], E. Kendziorra[22], M. Kerschhaggl[7], D. Khangulyan[1], B. Khélifi[15], D. Keogh[4], Nu. Komin[9], K. Kosack[1], G. Lamanna[16], J.-P. Lenain[8], T. Lohse[7], V. Marandon[17], J. M. Martin[8], O. Martineau-Huynh[14], A. Marcowith[19], D. Maurin[14], T. J. L. McComb[4], C. Medina[8], R. Moderski[11], E. Moulin[9], M. Naumann-Godo[15], M. de Naurois[14], D. Nedbal[24], D. Nekrassov[1], J. Niemiec[18], S. J. Nolan[4], S. Ohm[1], J.-F. Olive[5], E. de Oña Wilhelmi[17], K. J. Orford[4], J. L. Osborne[4], M. Ostrowski[25], M. Panter[1], G. Pedaletti[6], G. Pelletier[13], P.-O. Petrucci[13], S. Pita[17], G. Pühlhofer[6], M. Punch[17], A. Quirrenbach[6], B. C. Raubenheimer[12], M. Raue[20], S. M. Rayner[4], M. Renaud[1], F. Rieger[1,30], J. Ripken[20], L. Rob[24], S. Rosier-Lees[16], G. Rowell[26], B. Rudak[11], C. B. Rulten[4], J. Ruppel[27], V. Sahakian[3], A. Santangelo[22], R. Schlickeiser[27], F. M. Schöck[10], R. Schröder[27], U. Schwanke[7], S. Schwarzburg[22], S. Schwemmer[6], A. Shalchi[27], J. L. Skilton[21], H. Sol[8], D. Spangler[4], L. Stawarz[25], R. Steenkamp[28], C. Stegmann[10], G. Superina[15], P. H. Tam[6], J.-P. Tavernet[14], R. Terrier[17], O. Tibolla[6], C. van Eldik[1], G. Vasileiadis[19], C. Venter[12], J. P. Vialle[16], P. Vincent[14], M. Vivier[9,32], H. J. Völk[1], F. Volpe[15,30], S. J. Wagner[6], M. Ward[4], A. A. Zdziarski[11], and A. Zech[8]

[1] Max-Planck-Institut für Kernphysik, P.O. Box 103980, D 69029 Heidelberg, Germany
[2] Dublin Institute for Advanced Studies, 5 Merrion Square, Dublin 2, Ireland
[3] Yerevan Physics Institute, 2 Alikhanian Brothers St., 375036 Yerevan, Armenia
[4] University of Durham, Department of Physics, South Road, Durham DH1 3LE, UK
[5] Centre d'Etude Spatiale des Rayonnements, CNRS/UPS, 9 av. du Colonel Roche, BP 4346, F-31029 Toulouse Cedex 4, France
[6] Landessternwarte, Universität Heidelberg, Königstuhl, D 69117 Heidelberg, Germany
[7] Institut für Physik, Humboldt-Universität zu Berlin, Newtonstr. 15, D 12489 Berlin, Germany
[8] LUTH, Observatoire de Paris, CNRS, Université Paris Diderot, 5 Place Jules Janssen, 92190 Meudon, France
[9] IRFU/DSM/CEA, CE Saclay, F-91191 Gif-sur-Yvette, Cedex, France
[10] Universität Erlangen-Nürnberg, Physikalisches Institut, Erwin-Rommel-Str. 1, D 91058 Erlangen, Germany
[11] Nicolaus Copernicus Astronomical Center, Warsaw, Poland
[12] Unit for Space Physics, North-West University, Potchefstroom 2520, South Africa
[13] Laboratoire d'Astrophysique de Grenoble, INSU/CNRS, Université Joseph Fourier, BP 53, F-38041 Grenoble Cedex 9, France
[14] LPNHE, Université Pierre et Marie Curie Paris 6, Université Denis Diderot Paris 7, CNRS/IN2P3, 4 Place Jussieu, F-75252, Paris Cedex 5, France
[15] Laboratoire Leprince-Ringuet, Ecole Polytechnique, CNRS/IN2P3, F-91128 Palaiseau, France
[16] Laboratoire d'Annecy-le-Vieux de Physique des Particules, CNRS/IN2P3, 9 Chemin de Bellevue-BP 110 F-74941 Annecy-le-Vieux Cedex, France
[17] Astroparticule et Cosmologie (APC), CNRS, Universite Paris 7 Denis Diderot, 10, rue Alice Domon et Leonie Duquet, F-75205 Paris Cedex 13, France
[18] Instytut Fizyki Jądrowej PAN, ul. Radzikowskiego 152, 31-342 Kraków, Poland
[19] Laboratoire de Physique Théorique et Astroparticules, CNRS/IN2P3, Université Montpellier II, CC 70, Place Eugène Bataillon, F-34095 Montpellier Cedex 5, France
[20] Universität Hamburg, Institut für Experimentalphysik, Luruper Chaussee 149, D 22761 Hamburg, Germany
[21] School of Physics and Astronomy, University of Leeds, Leeds LS2 9JT, UK
[22] Institut für Astronomie und Astrophysik, Universität Tübingen, Sand 1, D 72076 Tübingen, Germany
[23] Toruń Centre for Astronomy, Nicolaus Copernicus University, Toruń, Poland
[24] Institute of Particle and Nuclear Physics, Charles University, V Holesovickach 2, 180 00 Prague 8, Czech Republic
[25] Obserwatorium Astronomiczne, Uniwersytet Jagielloński, Kraków, Poland
[26] School of Chemistry and Physics, University of Adelaide, Adelaide 5005, Australia
[27] Institut für Theoretische Physik, Lehrstuhl IV: Weltraum und Astrophysik, Ruhr-Universität Bochum, D 44780 Bochum, Germany
[28] University of Namibia, Private Bag 13301, Windhoek, Namibia
Received 2008 August 27; accepted 2008 September 15; published 2009 January 9

ABSTRACT

A search for a dark matter (DM) annihilation signal into γ-rays toward the direction of the Canis Major (CMa) overdensity is presented. The nature of CMa is still controversial and one scenario represents it as a dwarf galaxy, making it an interesting candidate for DM annihilation searches. A total of 9.6 hr of high-quality data were collected with the H.E.S.S. array of Imaging Atmospheric Cherenkov Telescopes, and no evidence for a very high energy γ-ray signal is found. Upper limits on the CMa dwarf galaxy mass of the order of 10^9 $M_\odot$ are derived at the 95% confidence level (CL) assuming neutralino masses in the range 500 GeV–10 TeV and relatively large annihilation cross sections. Constraints on the velocity-weighted annihilation cross section $\langle \sigma v \rangle$ are calculated for specific weakly interacting massive-particle scenarios, using a Navarro–Frenk–White model for the DM halo profile and taking advantage of

numerical simulations of hierarchical structure formation. Assuming a total halo mass of $3 \times 10^8\ M_\odot$, 95% CL exclusion limits of the order of 5×10^{-24} cm^3 s^{-1} are reached in the 500 GeV–10 TeV DM particle mass interval.

Key words: dark matter – galaxies: dwarf – gamma rays: observations

Online-only material: color figure

1. INTRODUCTION

It is widely believed that around one-third of the energy content of the Universe is made of cold matter, of which only a small fraction is luminous and is of baryonic origin. In the framework of the cold dark matter (CDM) scenarios, most of the matter is composed of nonbaryonic, weakly interacting massive particles (WIMPs). The standard model of particle physics does not provide a natural and suitable candidate for the dark matter (DM) particle, and many theories beyond the standard model have been proposed to explain its origin and properties (see Bertone et al. 2005 for a recent review). In various models, the self-annihilation of WIMPs gives a γ-ray continuum emission resulting from the hadronization of primary annihilation products. The spectral features of such a DM annihilation radiation might help to distinguish it from ordinary astrophysical sources (Bergström et al. 2005a, 2005b). The indirect detection of DM through very high energy (VHE) γ-rays is one of the best ways to probe the astrophysical nature of the DM, and the High Energy Stereoscopic System (H.E.S.S.), dedicated for detection of VHE γ-rays in the 100 GeV–10 TeV energy regime, is an interesting instrument for this purpose.

Many astrophysical objects, ranging from DM clumps to galaxy clusters are expected to lead to DM particle annihilation signals detectable with sufficiently sensitive instruments. Regions of high concentration of DM are good candidates to search for such annihilations, and the Galactic Centre (GC) was the first to be considered. H.E.S.S. observations of the GC region (Aharonian et al. 2004) revealed a source of VHE γ-ray emission (H.E.S.S. J1745-290) but ruled out the bulk of the signal as of DM origin (Aharonian et al. 2006c). Prospects for indirect detection in the elliptical galaxy M87 at the center of the Virgo cluster were also investigated. The time variability of the VHE γ-ray signal observed by H.E.S.S. (Aharonian et al. 2006a) gave clear evidence that the signal was not of a sole DM origin. There are also other candidates with high DM density in relative proximity that might lead to detectable DM annihilation signals. Satellite dwarf galaxies of the Milky Way (MW), such as Sagittarius (Sgr), Draco, or Canis Major (CMa), are popular targets, owing to their relatively low astrophysical background (Evans et al. 2004). Indeed, dwarf spheroidal (dSph) galaxies usually consist of stellar populations with no hot or warm gas and no cosmic rays, and are among the most extreme DM-dominated environments. A null result concerning the search for DM toward the Sgr dSph direction was published by the H.E.S.S. collaboration (Aharonian et al. 2008). Constraints on the parameter spaces of two popular WIMP models, namely the *R*-parity conserving Minimal Supersymmetric extension of the Standard Model (MSSM) and Kaluza-Klein (KK) scenarios with *K*-parity conservation, were derived. A null result was also established by the MAGIC collaboration (Albert et al. 2008) and the WHIPPLE collaboration (Wood et al. 2008), when searching for a DM annihilation signal toward the Draco dwarf galaxy. Upper limits on the velocity-weighted annihilation cross section of a DM particle were derived in the framework of minimal SUper GRAvity (mSUGRA) models and MSSM models.

This paper reports the search for a DM annihilation signal toward the direction of the CMa overdensity with the H.E.S.S. array of Cherenkov telescopes. The paper is organized as follows. In Section 2, the controversial nature of the CMa overdensity is briefly discussed, in Section 3, the analysis of the data is presented, while in Section 4, the predictions for DM annihilation into γ-rays in the CMa overdensity are discussed. Constraints on the WIMP velocity-weighted annihilation rate, as well as on the CMa total mass, are given.

2. A GALACTIC WARP OR THE RELIC OF A DWARF GALAXY?

Since its discovery (Martin et al. 2004), the nature of the CMa overdensity is the subject of many discussions over whether it is a dwarf galaxy or simply a part of the warped Galactic disk. According to Momany et al. (2006), the CMa overdensity simply reflects the warp and flare of the outer disk, a structure frequently observed in spiral galaxies such as the MW. The comparison of the kinematics of the CMa stars with those of the Galactic thick disk shows that the CMa stars do not have peculiar proper motions, which cast some doubts on the dSph nature of the CMa overdensity. The second scenario, which is of interest for the aim of this paper, considers this elliptical overdensity as the remnant of a disrupted dwarf galaxy that could have created the Monoceros "ring" structure (Martin et al. 2004). Indeed, numerical simulations show that such a structure can be explained by an in-plane accretion event, in which the remnant of the dwarf galaxy would have an orbital plane close to the Galactic plane. Another argument in favor of this scenario is that the CMa star populations do not exhibit the same properties as those in the disk since they have a relatively low metallicity (de Jong et al. 2007). In this case, the CMa star population would not belong to the Galactic disk, in contrast to what was found in Momany et al. (2006). The mass, luminosity, and characteristic dimensions of CMa appear quite similar to those of the Sgr dwarf galaxy. As for many dSphs, the CMa overdensity would thus be an interesting candidate for DM detection. In the remainder of the paper, the CMa object is assumed to be a dwarf galaxy.

The CMa overdensity is located toward the Galactic anticenter direction at roughly 8 kpc from the sun (Bellazinni et al. 2004) and is the closest observed dwarf galaxy. It is a very extended object ($\Delta l = 12^\circ, \Delta b = 10^\circ$) with a roundish core approximately centered at $l = 240^\circ$ and $b = -8^\circ$ according to various star surveys in this region (Martin et al. 2004; Martinez-Delgado et al. 2005). In contrast to the Sgr dSph, neither dispersion velocity measurements nor luminosity profiles are available, so an accurate modeling of the CMa DM halo profile is not possible. However, there are enough constraints to estimate the expected

[29] Supported by CAPES Foundation, Ministry of Education of Brazil.
[30] European Associated Laboratory for Gamma-Ray Astronomy, jointly supported by CNRS, and MPG.
[31] Also at UMR 7164 (CNRS, Université Paris VII, CEA, Observatoire de Paris).
[32] matthieu.vivier@cea.fr

γ-ray flux from DM particle annihilations in this object. The annihilation cross section is given by the particle physics model (see Section 4). Regarding the mass content of CMa, the narrow dispersion between the average mass values found for different dSph galaxies in the local group (Mateo 1998; Walker et al. 2007) is an indication that dSphs may possibly have a universal host halo mass (Dekel & Silk 1986). The mass of the CMa dwarf galaxy can then be inferred to be in the same range as the Sgr dwarf galaxy and many other dSphs so that the CMa total mass would range between 10^8 and 10^9 $M_\odot$ (Martin et al. 2004). For instance, Evans et al. (2004) gave a model where the CMa mass is taken as 3×10^8 $M_\odot$. The H.E.S.S. large field of view (FOV) covers a large part of the CMa core, optimizing the chances to see a potential DM annihilation signal.

3. H.E.S.S. OBSERVATIONS AND ANALYSIS

3.1. The H.E.S.S. Array of Imaging Atmospheric Cherenkov Telescopes

H.E.S.S. is an array of four Imaging Atmospheric Cherenkov Telecopes (IACTs; Hofmann et al. 2003) located in the Khomas Highland of Namibia at an altitude of 1800 m above the sea level. The instrument uses the atmosphere as a calorimeter and images electromagnetic showers induced by TeV γ-rays. Each telescope collects the Cherenkov light radiated by particle cascades in the air showers using a large mirror area of 107 m^2 and a camera of 960 photomultiplier tubes (PMTs). The four telescopes are placed in a square formation with a side length of 120 m. This configuration allows for an accurate reconstruction of the direction and energy of the γ-rays using the stereoscopic technique. The cameras cover a total FOV of 5° in diameter. The energy threshold of the H.E.S.S. instrument is approximately 100 GeV at zenith and its sensitivity allows to detect fluxes larger than 2×10^{-13} cm^{-2} s^{-1} above 1 TeV in 25 hr. More details on the H.E.S.S. experiment can be found in Aharonian et al. (2006b).

3.2. Data Processing

Observations of the CMa dwarf galaxy with H.E.S.S. were carried out in 2006 November with pointing angles close to the zenith and extending up to 20°. The nominal pointing direction was $l = 240.^\circ15$ and $b = -8.^\circ07$ in Galactic coordinates. The data were taken in a "wobble mode" with the telescope pointing typically shifted by $\pm$ 0.°7 from the nominal target position (Berge et al. 2007). The wobble observing mode reduces the systematic effects in the background estimates. The data set used for image analysis was selected using the standard quality criteria, excluding runs taken under bad or variable weather conditions. The CMa data set amounts to 9.6 hr of live time after quality selection. Two different techniques are combined for the data processing. The first technique computes the "Hillas geometrical moments" of the shower images to reconstruct shower geometry and energy, and to discriminate between γ-ray and hadronic events (Aharonian et al. 2005). The second technique uses a semianalytical model of air showers, which predicts the expected intensity in each camera pixel (de Naurois et al. 2003). Here, the shower direction, the impact point, and the primary particle energy are derived with a likelihood fit of the shower model to match the images. Standard cuts for γ-ray/hadron separations are derived from simulations. Both analyses provide an energy resolution of 15% and an angular resolution better than 0.°1. The combination of these two techniques, hereafter referred to as "Combined Hillas/Model analysis," uses a combined estimator (the so-called "Combined cut") and provides an improved background rejection. The background is estimated by following the template background method. This method uses events that fail the γ-ray selection cuts. The template background modeling is well suited for the detection of sources positioned anywhere in the FOV, as it estimates the background in each sky direction. More details on this background subtraction method are given in Rowell (2003). A charge cut of 60 photoelectrons on the image size is applied, as well as a cut on the primary interaction depth of particles to optimize the signal-to-noise ratio (S/N). Events that pass the analysis cuts are labeled as "γ candidates" and are stored in the so-called γ candidate map $n_\gamma^{\rm candidate}(l, b)$. Events that do not pass the analysis cuts are defined as "background events" and are stored in the so-called background map $n_{\rm bck}(l, b)$. Table 1 shows the different cut values used to select the γ-ray events.

Table 1
List of Cuts Used in the Analysis

Cut Name	γ-Event Cut Value
Combined cut	$\leqslant 0.7$
Image charge min.	$\geqslant 60$ photoelectrons
Reconstructed shower depth min. (rad. length)	-1
Reconstructed shower depth max. (rad. length)	4
Reconstructed nominal distance	$\leqslant 2.^\circ5$
Reconstructed event telescope multiplicity	$\geqslant 2$

Notes. The shower depth is the reconstructed primary interaction depth of the particles. The nominal distance is the angular distance of the image barycenter to the center of the camera.

The $2.^\circ5 \times 2.^\circ5$ excess sky map is obtained by the following equation:

$$n_\gamma^{\rm excess}(l, b) = n_\gamma^{\rm candidate}(l, b) - \alpha(l, b) \times n_{\rm bck}(l, b), \quad (1)$$

where $\alpha(l, b)$ refers to the template normalization factor as described in Rowell (2003). To search for a γ-ray signal, the raw fine-binned maps are integrated with a 0.°1 radius around each point to match the H.E.S.S. angular resolution, resulting in new oversampled maps of gamma-ray candidates and background events, and a corresponding gamma-ray excess map. Using the prescription of Li & Ma (1983) to derive the significance for each point of the oversampled map on the basis of the gamma-ray candidate and background counts and the template normalization factor, no significant excess is found at the target position or at other points in the FOV (Figure 1, left panel). The distribution of significances for the entire map is shown in the right panel of Figure 1 and is fully consistent with statistical fluctuations of the background signal. As the excess map does not show any signal, an upper limit on the number of gamma-ray events for each point in the map can be derived using the method of Feldman & Cousins (1998). The uncorrelated γ candidate and normalized background maps, plotted on a $0.^\circ2 \times 0.^\circ2$ grid with bins not smaller than the H.E.S.S. angular resolution, are used for the upper limit calculations.

4. PREDICTIONS FOR DARK MATTER ANNIHILATIONS IN THE CMA OVERDENSITY

The DM particles are expected to annihilate into a continuum of γ-rays through various processes such as the hadronization of quark final states, hadronic decay of τ leptons, and subsequent decay of mesons. Two DM candidates are commonly discussed in the literature: the so-called neutralino arising in supersymmetric extensions of the standard model (SUSY; Jungman

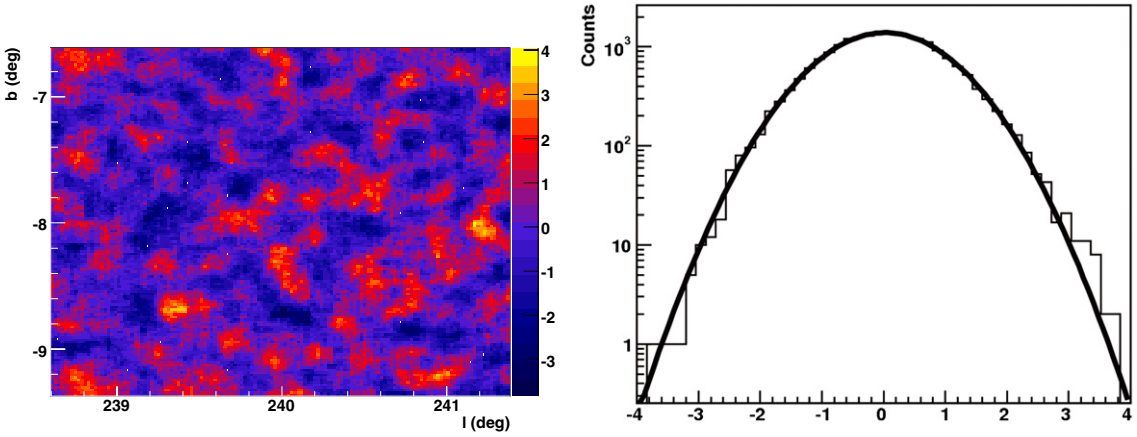

Figure 1. Left: Significance map corresponding to the excess map computed in the analysis (see text), calculated according to the Li & Ma method (Li & Ma 1983). Right: Significance distribution derived from the significance map. The solid line shows the Gaussian fit. The mean value is 0.01 ± 0.004 and the corresponding variance is 1.000 ± 0.005.

et al. 1996) and the first excitation of the hypercharge gauge boson in Universal Extra Dimension (UED) theories called the $B^{(1)}$ particle (Servant & Tait 2003). Typical masses for these DM candidates range from 50 GeV to several TeV. The value of the annihilation cross section is constrained to give a thermal relic abundance of WIMPs that is in agreement with the *Wilkinson Microwave Anisotropy Probe*+Sloan Digital Sky Survey (*WMAP*+SDSS) derived value (Tegmark et al. 2006). The velocity-weighted annihilation cross sections can be as low as 10^{-30} cm^3 s^{-1}, for scenarios involving co-annihilation processes, and as high as 10^{-25} cm^3 s^{-1}.

The expected flux ϕ_γ of γ-rays from WIMP annihilations occurring in a spherical dark halo is commonly written as a product of a particle physics term ($\mathrm{d}\Phi^{\mathrm{PP}}/\mathrm{d}E_\gamma$) and an astrophysics term (f^{AP}):

$$\phi_\gamma = \frac{\mathrm{d}\Phi^{\mathrm{PP}}}{\mathrm{d}E_\gamma} \times f^{\mathrm{AP}}. \quad (2)$$

The expected number of γ-ray is then given by

$$N_\gamma = T_{\mathrm{ON}} \times \int_0^{m_{\mathrm{DM}}c^2} \overline{A_{\mathrm{eff}}}(E_\gamma)\phi_\gamma(E_\gamma)\mathrm{d}E_\gamma, \quad (3)$$

where T_{ON} denotes the on-source exposure time, which depends on the pointing direction, and $\overline{A_{\mathrm{eff}}}(E_\gamma)$, the averaged H.E.S.S. acceptance during data collection. The velocity-weighted cross sections for WIMP annihilation $\langle\sigma v\rangle$ and the WIMP mass are fixed to compute the particle physics term in Equation (2):

$$\frac{\mathrm{d}\Phi^{\mathrm{PP}}}{\mathrm{d}E_\gamma} = \frac{\langle\sigma v\rangle}{4\pi m_{\mathrm{DM}}^2}\left[\frac{\mathrm{d}N}{\mathrm{d}E_\gamma}\right]_{\mathrm{DM}}, \quad (4)$$

where $(\mathrm{d}N/\mathrm{d}E_\gamma)_{\mathrm{DM}}$ is the γ-ray spectrum originating for DM particle annihilation. The shape of the continuum γ-ray spectrum, predicted in the framework of the phenomenological MSSM (pMSSM), depends on the model in a complicated way. A simplified parametrization of this shape, for higgsino-like neutralinos mainly annihilating via pairs of W and Z gauge bosons, was taken from Bergström et al. (1998). In the case of KK $B^{(1)}$ particle annihilations, the branching ratios to final states are independent of the WIMP mass. The differential photon continuum has been simulated with the PYTHIA package (Sjöstrand et al. 2003) using branching ratios from Servant & Tait (2003).

The astrophysics term f^{AP} illustrates the DM concentration dependence of the expected γ-ray flux toward the pointed source:

$$f^{\mathrm{AP}} = \int_{\Delta\Omega}\int_{\mathrm{los}} \rho^2(l)\mathrm{d}l\mathrm{d}\Omega, \quad (5)$$

where $\rho(l)$ is the mass density profile of the CMa dwarf galaxy and $\Delta\Omega$ is the detection solid angle ($\Delta\Omega = 10^{-5}$ sr, corresponding to the integration radius of 0.°1).

4.1. Model of the CMa Dark Matter Halo within the ΛCDM Cosmology

The purpose of this section is to explain how the astrophysical term f^{AP} (Equations (2) and (5)) was calculated as a function of the total CMa dark halo mass. The estimate of the astrophysical term f^{AP} relies on the modeling of the CMa DM mass distribution. Observationally, the DM mass content of dSph galaxies can be derived by using velocity dispersion measurements of their stellar population and their luminosity profile. The comparison between models and observations can constrain the parameters of their assumed density profiles. In the case of the CMa dSph, the lack of available observational data prevents the modeling of its density profile in the same way as in the literature (Evans et al. 2004; Colafrancesco et al. 2007; Aharonian et al. 2008).

In the absence of observational data, a standard cusped Navarro–Frenk–White (NFW) halo (Navarro et al. 1997) was assumed to model the CMa dwarf mass distribution:

$$\rho_{\mathrm{cusped}}(r) = \frac{\rho_0}{\frac{r}{r_{\mathrm{s}}}\left(1+\frac{r}{r_{\mathrm{s}}}\right)^2}, \quad (6)$$

where ρ_0 is the overall normalization and r_{s} the scale radius. The parameters ρ_0 and r_{s} determining the shape of the profile, and the halo virial mass M_{vir} are found by solving the following system of three equations:

$$M_{\mathrm{vir}} = \int_0^{R_{\mathrm{vir}}} \rho_{\mathrm{cusped}}(r)\mathrm{d}^3\vec{r}, \quad (7)$$

$$M_{\mathrm{vir}} = \frac{4\pi}{3}\rho_{200} \times R_{\mathrm{vir}}^3, \quad (8)$$

$$C_{\mathrm{vir}}(M_{\mathrm{vir}}, z) = \frac{c_0}{1+z} \times \left[\frac{M_{\mathrm{vir}}}{10^{14}h^{-1}M_\odot}\right]^\alpha, \quad (9)$$

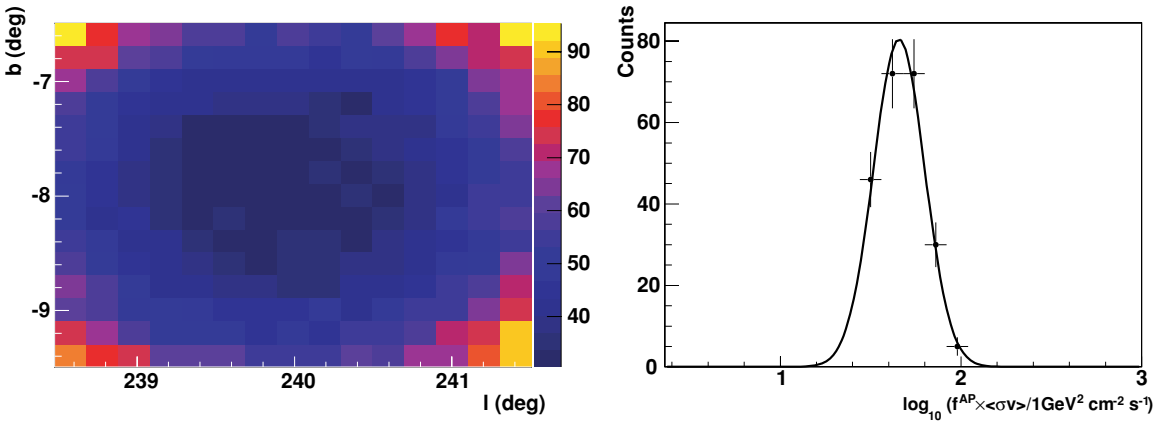

Figure 2. Left: 95% CL upper limit map on the value of $\langle\sigma v\rangle \times f^{\rm AP}$ derived for a 1 TeV neutralino (see text). Right: Distribution of the 95% CL $\langle\sigma v\rangle \times f^{\rm AP}$ upper limits logarithm derived with the upper limit map from the left panel. The solid line shows the Gaussian fit. The mean value is 1.66 ± 0.01 and the corresponding variance is 0.14 ± 0.01.

Table 2
Structural Parameters of NFW Dark Matter Halos and Associated $f^{\rm AP}$ Values Derived with the Procedure Described in the Text, for Three Different Virial Masses

$M_{\rm vir}$ ($M_\odot$)	ρ_0 ($10^8\ M_\odot\ {\rm kpc}^{-3}$)	$r_{\rm s}$ (kpc)	$r_{\rm t}$ (kpc)	$M(r \leqslant r_{\rm t})$ ($M_\odot$)	$f^{\rm AP}$ ($10^{24}\ {\rm GeV}^2\ {\rm cm}^{-5}$)
10^6	4.7	0.04	0.28	3.9×10^5	0.24
10^8	1.3	0.28	1.17	3.1×10^7	2.2
10^{10}	0.39	2.08	4.15	1.9×10^9	12

where $R_{\rm vir}$ is the halo virial radius. The virial radius is computed given the virial mass $M_{\rm vir}$ and is defined as the radius within which the mean density equals ρ_{200} ($\rho_{200} = 200 \times \rho_{\rm c}$, where $\rho_{\rm c}$ is the critical density of the universe[33]).

Equation (9) relates the concentration parameter $C_{\rm vir}$ to the virial mass. The concentration parameter is defined as the ratio of the virial radius to the scale radius $R_{\rm vir}/r_{\rm s}$ in the case of a NFW profile. The relation between $C_{\rm vir}$ and $M_{\rm vir}$ is not well known and was studied in various simulations of structure formation. Equation (9) is used following the halo concentration fit of Dolag et al. (2004), which is in good agreement with most of N-body simulations proposed in the literature (see Bullock et al. 2001 and Eke et al. 2001 as examples). In Equation (9), z denotes the redshift and h the present-day normalized Hubble expansion rate. The parameters of the halo concentration fit, c_0 and α, depend on the cosmological scenario ($c_0 = 9.6$ and $\alpha = -0.1$ in a ΛCDM cosmology). The CMa dSph galaxy is located close to the Galactic disk and suffers from strong tidal disruptions. A reasonably good estimator of its total dark halo mass is then the mass enclosed inside its tidal radius rather than its virial mass. The tidal radius of the CMa dwarf galaxy is calculated via the Roche criterion:

$$\frac{M_{\rm dSph}(r_{\rm t})}{r_{\rm t}^3} = \frac{M_{\rm MW}(d - r_{\rm t})}{(d - r_{\rm t})^3}, \qquad (10)$$

where d is the distance of CMa to the center of the MW. $M_{\rm MW}$(r) denotes the mass of the MW galaxy enclosed in a sphere of radius r. A NFW profile for the MW halo is considered with a concentration parameter equal to 10 and a virial mass of $10^{12}\ M_\odot$. The total mass of the dSph galaxy is computed by iterative tidal stripping, first inserting $M_{\rm vir}$ in Equation (10) and successively computing the total halo mass (using Equation (7)) and the tidal radius (using Equation (10)), until the convergence of the procedure is reached. The question is now whether or not tidal forces significantly remodel the internal structure of tidally affected dSph. Discrepant results have been reported in the literature regarding this question (Reed et al. 2005; Stoehr et al. 2002). Here, it is assumed that tidal forces do not affect the inner part of the density profile so that the initial halo structural parameters are kept constant during the stripping procedure. The remaining mass is typically found to be an order of magnitude lower than the virial mass.

The astrophysical term $f^{\rm AP}$ can then be computed as a function of the halo mass by performing a line-of-sight (LOS) integration of the CMa dSph squared mass density, according to Equation (5). Table 2 shows the obtained NFW structural parameters for a sample of three dark matter halos with different virial masses. The integral of the squared mass density increases with the halo mass and the $f^{\rm AP}$ value for a dwarf galaxy of mass $10^8\ M_\odot$, located at a heliocentric distance of 8 kpc, is found to be in the right order of magnitude ($f^{\rm AP} \sim 10^{25}\ {\rm GeV}^2\ {\rm cm}^{-5}$) compared to Evans et al. (2004).

4.2. Halo-Independent Constraints on the Annihilation Signal

Using the upper limit γ map on the number of γ events derived with the γ candidate map and the normalized background map (see Section 3.2 for details), upper limits on the value of $\langle\sigma v\rangle \times f^{\rm AP}$ can be derived (Equations (2)–(4)) for various neutralino masses. As an example, the left panel of Figure 2 shows a sky map of the 95% confidence level (CL) upper limit values on $\langle\sigma v\rangle \times f^{\rm AP}$, computed within a pMSSM scenario for a 1 TeV higgsino-like neutralino annihilating in pairs of W and Z gauge bosons. The sensitivity is better toward the center of the FOV, because the H.E.S.S. acceptance decreases on the edges of the camera. H.E.S.S. is sensitive to $\langle\sigma v\rangle \times f^{\rm AP}$ values of the order of $10^2\ {\rm GeV}^2\ {\rm cm}^{-2}\ {\rm s}^{-1}$. Since the core of the CMa dSph can be anywhere in the FOV, one obtains a distribution of the $\langle\sigma v\rangle \times f^{\rm AP}$ upper limits over the FOV. As shown by the right panel of Figure 2, this distribution is well fitted by a Gaussian curve. The mean value can be taken as the $\langle\sigma v\rangle \times f^{\rm AP}$ 95% CL upper-limit reference value, and the corresponding 1σ error bar reflects the uncertainties associated with it.

Using this procedure, an exclusion curve in the plane ($\langle\sigma v\rangle \times f^{\rm AP}$, $m_{\rm DM}$) can be derived. The corresponding curve is shown in the left panel of Figure 3. The gray shaded areas

[33] http://pdg.lbl.gov

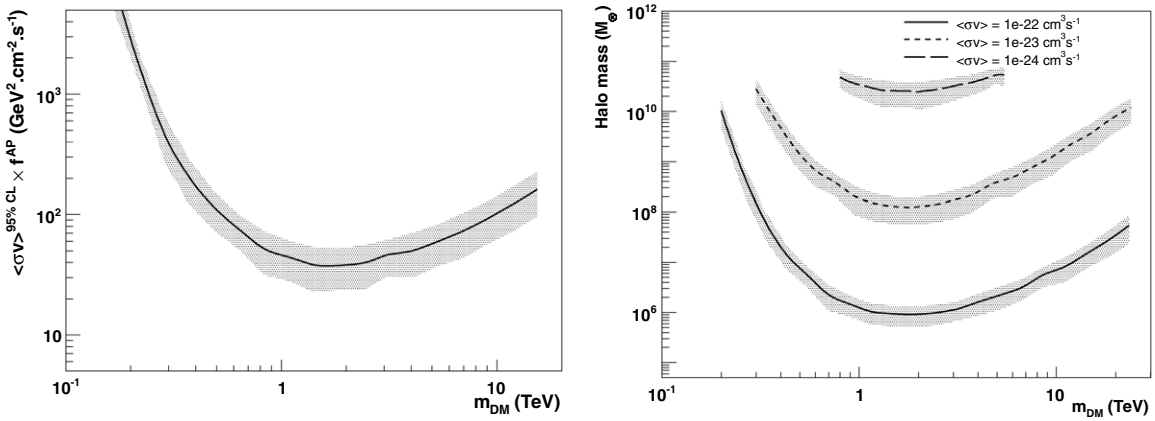

Figure 3. Left: Upper limits at 95% CL on the value of $\langle \sigma v \rangle \times f^{\rm AP}$ as a function of the DM particle mass in the framework of pMSSM scenarios. Right: Upper limits at 95% CL on the CMa total mass vs. the DM particle mass for different annihilation cross sections in pMSSM scenarios. The shaded area represents the error bars issued from the 1σ error on the $\langle \sigma v \rangle \times f^{\rm AP}$ distribution Gaussian fits (see text for details).

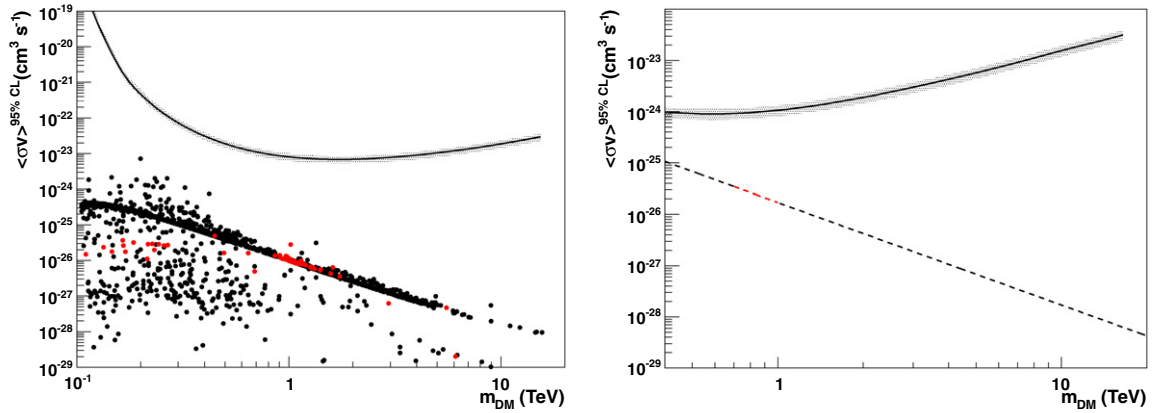

Figure 4. Upper limits at 95% CL on the velocity-weighted cross section as a function of the DM particle mass in the case of pMSSM (left panel) and KK (right panel) scenarios, for an assumed CMa total mass of $3 \times 10^8\ M_\odot$. The shaded area represents the 1σ error bars on $\langle \sigma v \rangle^{95\%\rm CL}$ (see text for details). Left: The pMSSM models are represented by black points, and those giving a CDM relic density in agreement with the measured *WMAP*+SDSS value are illustrated by red points. Right: The KK models are represented by the black dashed line, and those verifying the *WMAP*+SDSS constraint on $\Omega_{\rm CDM}h^2$ are labeled in red.

(A color version of this figure is available in the online journal.)

represent the 1σ uncertainties associated with the 1σ error bars on the $\langle \sigma v \rangle \times f^{\rm AP}$ 95% upper limit.

4.3. Sensitivity to the CMa Mass

As the $f^{\rm AP}$ factor is related to the CMa halo mass (see Section 4.1), an upper limit on the total CMa mass can be obtained using the previously derived exclusion curve on the $\langle \sigma v \rangle \times f^{\rm AP}$ quantity and assuming a fixed value for the annihilation cross section. WIMP velocity-weighted annihilation cross sections are expected to be of the order of weak-scale interaction cross sections. Exclusion curves in the plane $\left(M_{\rm CMa}^{95\%\rm CL}, m_{\rm DM}\right)$ are then plotted for different annihilation cross sections within pMSSM scenarios, using the parametrization of Bergström et al. (1998) for the γ-ray annihilation spectrum. The corresponding curves are shown in the right panel of Figure 3. The gray shaded areas represent the 1σ uncertainties associated with the 1σ error bars on the $\langle \sigma v \rangle \times f^{\rm AP}$ 95% upper limit, as described in the previous section. Annihilation cross sections larger than 10^{-24} cm^3 s^{-1} are considered here. Lower cross sections would have been too small to constrain the CMa dSph mass; for example the excluded masses would have been of the order of a MW-sized galaxy for a typical velocity-weighted annihilation cross section of 3×10^{-26} cm^3 s^{-1}.

Table 3
Comparison Table of the NFW Structural Parameters of the CMa and Sgr dSph, with their Associated $f^{\rm AP}$ Values, Assuming for Both a Total Mass of $3 \times 10^8\ M_\odot$

	Heliocentric Distance (kpc)	ρ_0 ($10^8\ M_\odot$ kpc^{-3})	r_s (kpc)	$f^{\rm AP}$ (10^{24} GeV^2 cm^{-5})
CMa	8	1.1	0.55	5.9
Sgr	24	1.4	0.62	2.2

Table 4
Region of the pMSSM Parameter Space Scanned to Generate the Models

pMSSM Parameters
$100\ {\rm GeV} \leqslant \mu \leqslant 30\ {\rm TeV}$
$100\ {\rm GeV} \leqslant m_0 \leqslant 1\ {\rm TeV}$
$1.2 \leqslant \tan\beta \leqslant 60$
$10\ {\rm GeV} \leqslant M_2 \leqslant 50\ {\rm TeV}$
$-3\ {\rm TeV} \leqslant A_{\rm t,b} \leqslant 3\ {\rm TeV}$
$50\ {\rm GeV} \leqslant M_{\rm A} \leqslant 10\ {\rm TeV}$

Note. A set of free parameters in the considered range is associated with a pMSSM model.

4.4. Sensitivity to the Annihilation Cross-Section of WIMP Candidates

In this part, the CMa total mass is fixed to be $3 \times 10^8\ M_\odot$ and the corresponding value of the astrophysical contribution $f^{\rm AP}$ in the expected γ-ray flux is computed following the procedure described in Section 4.1. Table 3 compares the value of the CMa dSph and Sgr dSph structural parameters[34] assuming a NFW profile. The contribution of the astrophysical term $f^{\rm AP}$ is larger for the CMa dSph than for the Sgr dSph because CMa is closer to the Sun. Limits on the velocity-weighted annihilation cross section $\langle \sigma v \rangle^{95\%\rm CL}$ can then be derived as a function of the DM particle mass. Limits are computed in the framework of SUSY and KK models.

The SUSY parameters are computed with the micrOMEGAs v1.37 software package (Belanger et al. 2004). Phenomenological MSSM scenarios have been considered. They are characterized by seven independent parameters: the higgsino mass parameter μ, the common sfermions scalar mass m_0, the Higgs fields vacuum expectation value ratio $\tan\beta$, the gaugino mass M_2, the trilinear couplings $A_{\rm t}$ and $A_{\rm b}$, and the CP-odd Higgs mass $M_{\rm A}$. Table 4 summarizes the region of the pMMSM parameter space scanned to generate the models. The left panel of Figure 4 shows the H.E.S.S. exclusion limits on the velocity-weighted cross section. The black points illustrate the computed pMSSM scenarios and the red points represent those satisfying the *WMAP*+SDSS constraints on the CDM relic density $\Omega_{\rm CDM}h^2$ (Tegmark et al. 2006). The CDM relic density $\Omega_{\rm CDM}h^2$ is allowed to range between 0.09 and 0.11. The H.E.S.S. observations of the CMa dSph allows the exclusion of velocity-weighted cross sections of the order of 5×10^{-24} cm^3 s^{-1}, comparable with those derived for the Sgr dSph modeled with a cusped NFW profile. The limits obtained are an order of magnitude larger than the velocity-weighted annihilation cross sections of higgsino-like neutralinos.

In the case of KK scenarios, predictions for the velocity-weighted cross section are computed with the formula given in Baltz & Hooper (2005). The expression of $\langle \sigma v \rangle$ is inversely proportional to the squared mass of the lightest Kaluza–Klein particle (LKP), namely the $B^{(1)}$ particle. Considered KK models that reproduce the CDM relic measured by *WMAP* and SDSS require a LKP mass ranging from 0.7 TeV to 1 TeV. The right panel of Figure 4 shows the H.E.S.S. limits obtained within these models. The H.E.S.S. observations do not constrain the KK velocity-weighted cross section.

5. CONCLUSIONS

The CMa overdensity is the subject of many debates over whether it is a dwarf galaxy or a warp and flare of the Galactic outer disk. Considering the first scenario, its relative proximity makes it potentially the best region for searches of a DM annihilation signal. However, the lack of observational data prevents the precise modeling of its density profile. Assuming a NFW profile and a mass content of $3 \times 10^8\ M_\odot$ within its tidal radius, typical of dwarf galaxies, H.E.S.S. is close enough to exclude a few pMMSM scenarios with higgsino-like neutralinos, but does not reach the necessary sensitivity to test models compatible with the *WMAP*+SDSS constraint on the CDM relic density. In the case of DM made of $B^{(1)}$ particle from KK models with extra dimensions, no constraints are obtained.

[34] The NFW structural parameters for the Sgr dSph galaxy were estimated in Evans et al. (2004) using the velocity dispersion measurements of the Draco dSph galaxy whereas those of the CMa dSph are derived using numerical simulation results (see Section 4.1).

The support of the Namibian authorities and of the University of Namibia in facilitating the construction and operation of H.E.S.S. is gratefully acknowledged. The support by the German Ministry for Education and Research (BMBF), the Max Planck Society, the French Ministry for Research, the CNRS-IN2P3 and the Astroparticle Interdisciplinary Programme of the CNRS, the U.K. Particle Physics and Astronomy Research Council (PPARC), the IPNP of the Charles University, the Polish Ministry of Science and Higher Education, the South African Department of Science and Technology and National Research Foundation, and by the University of Namibia is also greatly acknowledged. We appreciate the excellent work of the technical support staff in Berlin, Durham, Hamburg, Heidelberg, Palaiseau, Paris, Saclay, and Namibia in the construction and operation of the equipment.

REFERENCES

Aharonian, F., et al. 2004, A&A, 425, L13
Aharonian, F., et al. 2005, A&A, 430, 865
Aharonian, F., et al. 2006a, Science, 314, 1424
Aharonian, F., et al. 2006b, A&A, 457, 899
Aharonian, F., et al. 2006c, Phys. Rev. Lett., 97, 221102
Aharonian, F., et al. 2008, Astropart. Phys, 29, 55
Albert, J., et al. 2008, ApJ, 679, 428
Baltz, E., & Hooper, D. 2005, J. Cosmol. Astropart. Phys., 0507, 001
Belanger, G., Boudjema, F., Pukhov, A., & Semenov, A. 2004, arXiv:hep-ph/0405253
Bellazinni, M., et al. 2004, MNRAS, 354, 1263
Berge, D., Funk, S., & Hinton, J. 2007, A&A, 466, 1219
Bergström, L., Bringmann, T., Eriksson, M., & Gustafsson, M. 2005a, Phys. Rev. Lett., 94, 131301
Bergström, L., Bringmann, T., Eriksson, M., & Gustafsson, M. 2005b, Phys. Rev. Lett., 95, 241301
Bergström, L., Ullio, P., & Buckley, J. 1998, Astropart. Phys, 9, 137
Bertone, G., Hooper, D., & Silk, J. 2005, Phys. Rep., 405, 279
Bullock, J., et al. 2001, MNRAS, 321, 559
Colafrancesco, S., Profumo, S., & Ullio, P. 2007, Phys. Rev. D., 75, 023513
de Jong, J. T. A., et al. 2007, ApJ, 662, 259
de Naurois, M., et al. 2003, in Proc. of the 28th ICRC 5, ed. T. Kajita et al. (Tokyo: Universal Academy Press), 2907
Dekel, A., & Silk, J. 1986, ApJ, 303, 39
Dolag, K., et al. 2004, A&A, 416, 853
Eke, V. R., Navarro, J. F., & Steinmetz, M. 2001, ApJ, 554, 114
Evans, N. W., Ferrer, F., & Sarkar, S. 2004, Phys. Rev. D., 69, 123501
Feldman, G., & Cousins, R. 1998, Phys. Rev. D., 57, 3873
Hofmann, W., et al. 2003, in Proc. of the 28th ICRC 1, ed. T. Kajita et al. (Tokyo: Universal Academy Press), 2811
Jungman, G., Kamionkowski, K., & Griest, K. 1996, Phys. Rep., 276, 195
Li, T., & Ma, Y. 1983, ApJ, 272, 317
Martin, N. F., et al. 2004, MNRAS, 348, 12
Martinez-Delgado, D., et al. 2005, ApJ, 633, 205
Mateo, M. 1998, ARA&A, 36, 435
Momany, Y., et al. 2006, A&A, 451, 515
Navarro, J., Frenk, C., & White, S. 1997, ApJ, 490, 493
Reed, D., et al. 2005, MNRAS, 357, 82
Rowell, G. P. 2003, A&A, 410, 389
Servant, G., & Tait, T. 2003, Nucl. Phys. B., 650, 391
Sjöstrand, T., Lönnblad, L., Mrenna, S., & Skands, P. 2003, PYTHIA 6.3, arXiv:hep-ph/0308153
Stoehr, F., et al. 2002, MNRAS, 335, L84
Tegmark, M., et al. 2006, Phys. Rev. D., 74, 123507
Walker, M. G., et al. 2007, ApJ, 667, L53
Wood, M., et al. 2008, ApJ, 678, 594